Biology of Human Tumors

Clinical Cancer Research

miR-154* and miR-379 in the DLK1-DIO3 MicroRNA Mega-Cluster Regulate Epithelial to Mesenchymal Transition and Bone Metastasis of Prostate Cancer

Murali Gururajan[1], Sajni Josson[1], Gina Chia-Yi Chu[1], Chia-Lun Lu[1], Yi-Tsung Lu[1], Christopher L. Haga[2], Haiyen E. Zhau[1], Chunyan Liu[1], Jake Lichterman[1], Peng Duan[1], Edwin M. Posadas[1], and Leland W.K. Chung[1]

Abstract

Purpose: MicroRNAs in the delta-like 1 homolog–deiodinase, iodothyronine 3 (DLK1-DIO3) cluster have been shown to be critical for embryonic development and epithelial to mesenchymal transition (EMT). DLK1-DIO3 cluster miRNAs are elevated in the serum of patients with metastatic cancer. However, the biologic functions of these miRNAs in the EMT and metastasis of cancer cells are poorly understood. We previously demonstrated the oncogenic and metastatic role of miR-409-3p/5p, a member of this cluster, in prostate cancer. In this study, we defined the role of miR-154* and miR-379, two key members of this cluster, in prostate cancer progression and bone metastasis in both cell line models and clinical specimens.

Experimental Design: Genetic manipulation of miR-154* and miR-379 was performed to determine their role in tumor growth, EMT, and bone metastasis in mouse models. We determined the expression of miR-154* in prostate cancer clinical samples and bone metastasis samples using *in situ* hybridization and quantum dot labeling.

Results: Elevated expression of miR-154* and miR-379 was observed in bone metastatic prostate cancer cell lines and tissues, and miR-379 expression correlated with progression-free survival of patients with prostate cancer. Intracardiac inoculation (to mimic systemic dissemination) of miR-154* inhibitor-treated bone metastatic $ARCaP_M$ prostate cancer cells in mice led to decreased bone metastasis and increased survival.

Conclusion: miR-154* and miR-379 play important roles in prostate cancer biology by facilitating tumor growth, EMT, and bone metastasis. This finding has particular translational importance because miRNAs in the DLK1-DIO3 cluster can be attractive biomarkers and possible therapeutic targets to treat bone metastatic prostate cancer. *Clin Cancer Res; 20(24); 6559–69. ©2014 AACR.*

Introduction

Cancer cells often undergo epithelial to mesenchymal transition (EMT) before metastasizing to distant organs. Cancer cells activate embryonic programs and pathways that partially maintain stem cell identity, often referred as "stemness." Recent studies suggest roles for miRNAs in both metastasis and cancer stem cell formation (1, 2). The miRNA members of the delta-like 1 homolog–deiodinase, iodothyronine 3 (DLK1-DIO3) clusters are activated in embryonic stem cells. During mouse embryogenesis, the miRNA members of the DLK1-DIO3 cluster have been shown to be elevated in the developing central nervous system, skeletal muscle, liver, and lung (3). Similarly, several transgenic mouse models of prostate, liver, and lung cancer also exhibit elevated levels of DLK1-DIO3 cluster miRNA members (4–8). The functions of many of these miRNAs within this imprinted region remain largely unexplored in cancer biology, specifically for EMT and cancer stemness.

Members of the DLK1-DIO3 cluster have been recently shown to be upregulated in the serum of patients with prostate cancer and lung cancer. Members of this cluster, including miR-379, miR-154*, and miR-409-3p, show increased levels in the circulating exosomes of patients with

[1]Uro-Oncology Research Program, Department of Medicine, Samuel Oschin Comprehensive Cancer Institute, Cedars-Sinai Medical Center, Los Angeles, California. [2]The Scripps Research Institute, Jupiter, Florida.

Note: Supplementary data for this article are available at Clinical Cancer Research Online (http://clincancerres.aacrjournals.org/).

M. Gururajan and S. Josson contributed equally to this article.

Corresponding Authors: Leland W.K. Chung, Cedars-Sinai Medical Center, 8750 Beverly Blvd, Los Angeles, CA 90048. Phone: 310-423-7622; Fax: 310-423-8543; E-mail: Leland.Chung@cshs.org; and Sajni Josson, sajnij@gmail.com; and Murali Gururajan, gururajanmurali@gmail.com

doi: 10.1158/1078-0432.CCR-14-1784

Translational Relevance

Currently there are no good biomarkers or therapy for prostate cancer bone metastasis. MicroRNAs in the delta-like 1 homolog–deiodinase, iodothyronine 3 (DLK1-DIO3) cluster located in human chromosome 14 have been shown to be critical for embryonic development and epithelial to mesenchymal transition (EMT) of embryonic cells. In this study, we identified a novel role for miR-154* and miR-379, two members of the DLK1-DIO3 cluster, in prostate tumor growth, EMT, stemness, and bone metastasis. Further, we demonstrate that miR-154* and other miRNA members are elevated in cell lines and bone metastasis tissues from patients with prostate cancer. Overexpression of miR-154* and miR-379 in benign prostate cancer cells promotes EMT, and inhibition of miR-154* and miR-379 results in decreased EMT and bone metastasis in experimental models. Thus, miR-154* and miR-379, already implicated in embryonic development, have a role in prostate cancer metastasis and could serve both as a novel biomarker and as a therapeutic target.

lung adenocarcinomas (9) and breast (10) and prostate (11) cancers. Our recent studies demonstrate the importance of miR-409-3p/5p in prostate cancer growth, EMT, and bone metastasis (12). In this study, we studied the role of miR-154* and miR-379, two key DLK1-DIO3 cluster miRNAs, in several EMT models of human prostate cancer. We demonstrated that these miRNAs modulate EMT and drive metastasis. Thus, these miRNAs are promising therapeutic targets for aggressive prostate cancer.

Materials and Methods

Cell culture

Three human prostate cancer bone metastatic progression models, $ARCaP_E$ and $ARCaP_M$ (13), LNCaP, and C4-2 (14), were used in our study. Prostate cancer cells and 293T cells were cultured in T-medium (GibcoBRL) supplemented with 5% heat-inactivated FBS (Bio-Whittaker) and 1% penicillin–streptomycin. All cells were tested for mycoplasma every three months and were negative. Small RNA preparations derived from embryonic stem cells and induced pluripotent stem cells (iPSC) were provided by Drs. Sareen and Svendsen of the Regenerative Medicine Institute at Cedars-Sinai Medical Center. Generation and characterization of these cells are described in Supplementary Materials and Methods.

miRNA expression

Quantitative real-time PCR. Cells were trypsinized and total miRNA was extracted using a mirVana miRNA isolation kit (Ambion). miRNA expression analysis by quantitative real-time PCR (qRT-PCR) was performed separately for each miRNA using specific primer sets (Applied Biosystems) as previously described (15). RNU6B was used for normalization.

mRNA analysis. Total RNA was isolated from confluent monolayers of cells using the RNeasy Mini Kit (Qiagen). cDNA was made using SuperscriptIII reverse transcriptase (Life Technologies). mRNA primers were designed and synthesized at Integrated DNA Technologies. mRNA expression levels were determined by qRT-PCR assays and SYBR Green Dye (Applied Biosystems). Samples were analyzed using the $\Delta\Delta C_t$ method and normalized to 18S ribosomal RNA.

MSKCC database analysis

The dataset was published by the Memorial Sloan Kettering Cancer Center (MSKCC) team (16) and was obtained from cBioPortal (17). The expression levels of miR-154 and miR-379 were analyzed along with the survival data in the dataset. For the survival analysis of miR-379, the expression levels of miR-379 in patients with nonmetastatic disease were compared with the median expression level of normal individuals. The disease-free survival of patients with miR-379 expression levels higher than normal individuals ($n = 29$) was compared with those with lower miR-379 expression levels ($n = 78$). A Kaplan–Meier survival curve was done by log-rank test between high and low expression groups. The expression levels of miR-154* were not available in the dataset. For the analysis of miR-154, the expression levels of normal healthy individuals ($n = 29$) were compared with the expression levels of patients with primary ($n = 99$) and metastatic prostate cancer ($n = 14$). Two-tailed Student *t* tests were done between the normal group and two primary and metastatic groups for analysis of the differential expression of miR-154.

3′UTR assay

Stromal antigen 2 (STAG2) mutant luciferase activity: 3′untranslated region (3′UTR) STAG2 luciferase construct (Switchgear genomics) was used as the wild-type (WT) construct and it was further mutated as described below. miR-154* mimic and control miRNA were transiently transfected along with the WT or mutant (STAG2) construct into these 293T cells, and luciferase activity was determined 24 hours later using the Lightswitch luciferase assay system (Switchgear Genomics).

3′UTR mutant constructs: Mutated 3′UTR luciferase constructs were produced by site-directed mutagenesis. Briefly, primer pairs with two sequential base pair mutations in the miRNA seed sequence of the 3′UTR were generated. Following PCR amplification, parental methylated template DNA was digested for 1 hour with *Dpn* I. Two microliter of the reaction was then transformed into XL-10 Gold bacteria. Sixteen hours after transformation, colonies were picked for liquid culture. Plasmid DNA was isolated by the Zyppy Plasmid Miniprep Kit according to the manufacturer's directions (Zymo Research). Mutations were confirmed by sequencing before proceeding with luciferase assays.

Primers

miR-154* Stag2 1	aactagaactgctgagaggactgtatatacaatttt-aaacctaagttgatttttttctc
miR-154* Stag2 2	gagaaaaaaaatcaacttaggtttaaaattgtatat-acagtcctctcagcagttctagtt

Lentiviral transduction

$ARCaP_E$ prostate cancer cell lines were transduced with lentivirus expressing control or miR-Zip-154* (miR-154*i) or miR-Zip-379 (miR-379i; System Biosciences) or cluster overexpression plasmid (custom made, miR-154*, miR-379, miR-409-3p/-5p) with GFP or control GFP plasmid. $ARCaP_M$ prostate cancer cell lines were transduced with lentivirus expressing cluster inhibitor plasmid (custom made) with GFP. Lentiviral preparation and transduction of cell lines were performed per the manufacturer's instructions (System Biosciences). GFP-positive cells were FACS sorted and cultured *in vitro* before experiments were performed.

Cell viability assay and invasion assays

Cell viability assays were performed using trypan blue staining. Cancer cell invasion was assayed in companion 24-well plates (Becton Dickinson Labware) with 8 μm porosity polycarbonate filter membranes as described previously (18).

Western analysis

Whole cell lysates from cell lines were prepared using a modified RIPA lysis buffer (50 mmol/L Tris HCl, 1% NP-40, 0.5% Na-deoxycholate, 0.1% SDS, 150 mmol/L NaCl, 1 mmol/L EDTA, 10% glycerol) supplemented with 1:100 dilution of the protease inhibitor cocktail and the tyrosine phosphatase inhibitor (Sigma). Proteins were then separated on 4% to 20% or 10% acrylamide gels and transferred to nitrocellulose membrane. Membranes were probed with STAG2 (Cell Signaling Technology) antibody. β-Actin (Sigma) was used as the normalization control.

In situ hybridization–quantum dots. Mouse tibia was formalin-fixed and paraffin-embedded. The miRNA *in situ* hybridization (ISH) protocol was followed per the manufacturer's instructions (Exiqon). The scramble and miR-154* probes were 5′-biotin labeled. The probes were linked to streptavidin-conjugated quantum dot (QD). Tissue sections were deparaffinized, treated with proteinase-K, and dehydrated. ISH was performed for 1 hour at 55°C, followed by washes and streptavidin blocking and a reaction with streptavidin-conjugated QD at a specified wavelength. The QD staining procedure was followed as previously described (19). Single QD labeling was performed, and scramble or miR-154* probes were labeled with 625-nm QDs. Images were taken at 40×. Hematoxylin and eosin staining was performed on subsequent tissue sections.

Human tissue array. A Gleason score tissue array was obtained from Vancouver Prostate Center. The use of tissue specimens was approved by the institutional review board of the Cedars-Sinai Medical Center (IRB# Pro21228). The tissues consisted of benign prostatic hyperplasia (BPH; $N = 4$), Gleason score 6 ($N = 12$), and Gleason 7 ($N = 7$). Each tissue had two sample cores. The tissue array was stained for H&E and graded by a pathologist to confirm the Gleason score. Single QD labeling was performed as previously mentioned (19). miR-154* was labeled with 625-nm QD, and signals were quantified as previously mentioned (19). The QD fluorescence intensity of each tissue section was determined and analyzed. Human prostate caner bone tissues were stained following the same procedure, except multiplexed ISH-QD was performed, where miR-154* (red) was stained first followed by miR-409-3p (green) or miR-409-5p (green) which was labeled with 565-nm QD.

In vivo metastasis study. All animal experiments were Institutional Animal Care and Use Committee approved and done in accordance with institutional guidelines. Luciferase-tagged $ARCaP_M$ control and $ARCaP_M$-154*i cells were injected intracardially as previously described (20) in SCID/beige mice (Charles River Laboratories; $N = 5$). Mice were imaged using *X*-ray and bioluminescence via the IVIS Lumina Imaging system. Mice were given near infrared (NIR) dye (IR783) 48 hours before euthanasia. The tumor-specific NIR dye was used to detect metastatic tumors in the mice.

Statistical analysis

Values were expressed as mean ± SD. All experiments were done in triplicates at least two independent times. Statistical analysis was performed using the Student *t* test or ANOVA. Values of $P < 0.05$ were considered to be statistically significant.

Results

miR-154* and miR-379 of the DLK1-DIO3 cluster are overexpressed in bone metastatic EMT models of human prostate cancer

We determined the levels of miR-154/154* and miR-379 in two bone metastatic models of prostate cancer, ARCaP, and LNCaP. Mesenchymal-type $ARCaP_M$ cells upon intracardiac inoculation or orthotopic implantation have 100% bone metastatic capability compared with their isogenic epithelial-type counterpart $ARCaP_E$ cells (13). Similarly, C4-2 prostate cancer cells have a high metastatic ability compared with their lineage-related LNCaP cells (21). Both miR-154* and miR-379 were elevated in $ARCaP_M$ cells compared with $ARCaP_E$ cells, and in C4-2 cells compared with LNCaP cells (Fig. 1A). We determined the expression of miR-154* in prostate cancer bone metastasis tissues by ISH-QD and observed higher expression in the metastatic prostate cancer cells (Fig. 1B). Previous studies demonstrated that several members of the DLK1-DIO3 miRNA cluster are elevated in human embryonic stem cells and iPSCs (22, 23). We measured the relative levels of these miRNAs in H9 embryonic stem cells and in iPSCs. Both H9 human embryonic stem cells and patient-derived iPS cells had elevated expression of miR-154* (Fig. 1C and D) but not miR-379 (23). We previously demonstrated that one of the predominant signaling pathways activated in prostate cancer bone

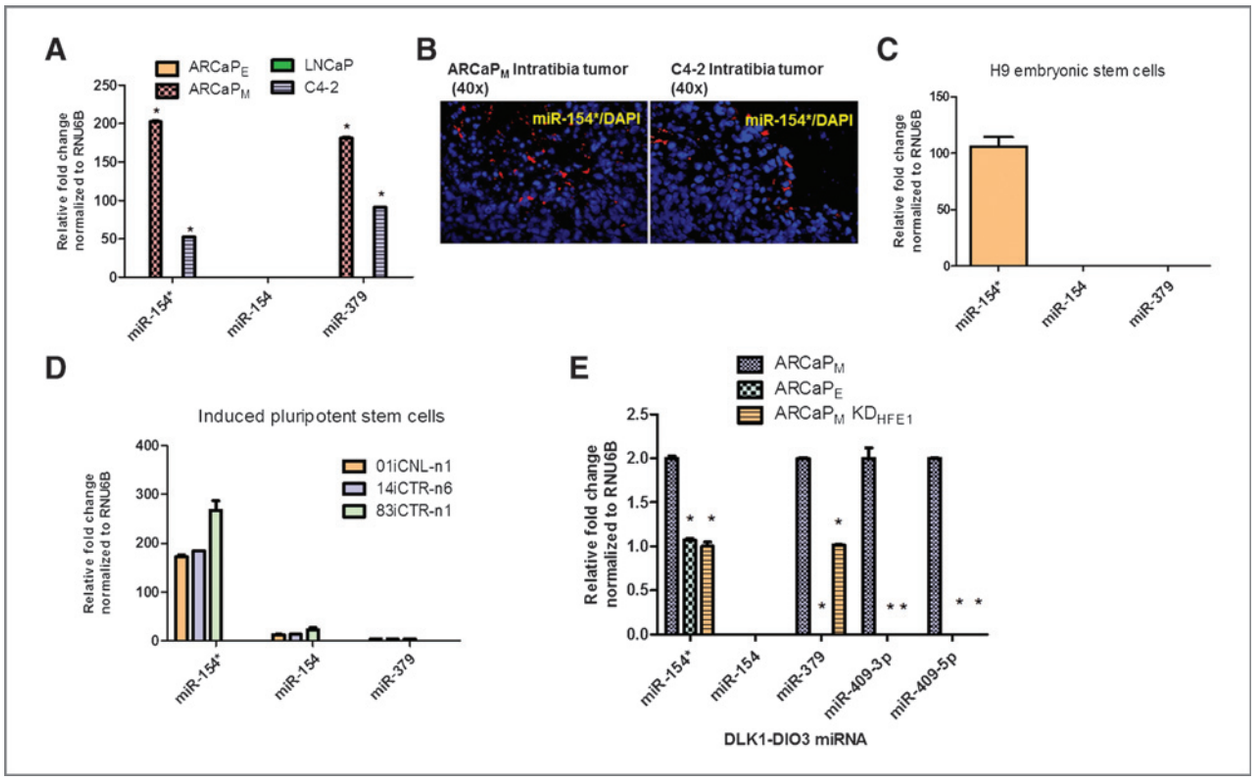

Figure 1. Members of the DLK1-DIO3 miRNA cluster (miR-154/154* and miR-379) are overexpressed in aggressive bone metastatic EMT models of human prostate cancer. A, miRNA expression of miR-154/154* and miR-379 in prostate cancer models (mesenchymal cells ARCaP$_M$ compared with ARCaP$_E$ and LNCaP versus C4-2 prostate cancer cells) by qRT-PCR analysis. B, miRNA-stained or miR-154*-stained prostate cancer mouse bone metastatic models (C4-2 and ARCaP$_M$ cells) assayed by ISH-QD analysis (magnification, ×40). miR-154* stained in red, nucleus stained with DAPI. C and D, miRNA expression of miR-154/154* and miR-379 in H9 embryonic stem cells and iPS cells by qRT-PCR. E, miRNA expression in EMT models of prostate cancer: mesenchymal cells (ARCaP$_M$) and epithelial cells (ARCaP$_E$ and ARCaP$_M$ KD$_{HFE1}$) as assayed by qRT-PCR. *, $P < 0.05$ was considered to be statistically significant by one-way ANOVA–Tukey analysis.

metastasis is the β2-microglobulin/hemochromatosis E (HFE) pathway (20, 24). Inhibition of either of these proteins results in reversal of EMT (20). We observed that ARCaP$_M$ HFE knockdown cells (ARCaP$_M$ KD^{HFE1}cells) had significantly decreased expression of miR-154* and miR-379 similar to the epithelial ARCaP$_E$ prostate cancer cells (Fig. 1E). In addition, other members, such as miR-409-3p/-5p of the DLK1-DIO3 cluster, were also decreased in ARCaP$_M$ HFE knockdown cells. These data together demonstrate that miR-154* and miR-379 are elevated in prostate cancer EMT and bone metastatic models.

Inhibition of miR-154* or miR-379 results in reversal of EMT (MET) of prostate cancer cells

To test the hypothesis whether miR-154* and miR-379 are involved in prostate cancer EMT, we transiently depleted miR-154* and miR-379 in ARCaP$_M$ and C4-2 cells using siRNA and determined the cell viability by the trypan blue exclusion test. miR-154* cells and miR-379 inhibited cells underwent cell death compared with control transfected cells in both of the prostate cancer cell line models studied (Fig. 2A). Next, we introduced an shRNA in the mesenchymal-type ARCaP$_M$ prostate cancer cells to generate miR-154* knockdown (ARCaP$_M$-154*i) or miR-379 knockdown (ARCaP$_M$-379i) cells. In addition, we used a scrambled shRNA to generate a control shRNA vector (ARCaP$_M$-C). Reduced expression of miR-154* was detected in the ARCaP$_M$-154*i cells by qRT-PCR analysis compared with the shRNA control vector ARCaP$_M$-C. Reduced expression of miR-379 was also observed in the ARCaP$_M$-379i cells by qPCR analysis compared with the ARCaP$_M$-C cells (Fig. 2B). RNU6B was used for normalization. The miR-154* target gene, stromal antigen 2 (STAG2), was measured in the knockdown cells (TargetScan v6.2). STAG2 is a tumor suppressor protein (25). The mRNA and protein expression of STAG2 was increased in the ARCaP$_M$-154*i cells compared with the control ARCaP$_M$ cells (Fig. 2C). We further tested if miR-154* directly binds to the 3′UTR of STAG2 using a luciferase reporter assay. Compared with control miRNA–treated cells, miR-154* mimic-treated cells had reduced basal luciferase activity (Fig. 2D). We mutated the 3′UTR of STAG2 at the miR-154* binding site and demonstrated restoration of luciferase activity in response to the miR-154* mimic (Fig. 2D). Interestingly, inhibition of miR-154* or miR-379 led to reversion of mesenchymal ARCaP$_M$ cells to an epithelial phenotype (Fig. 2E) accompanied by

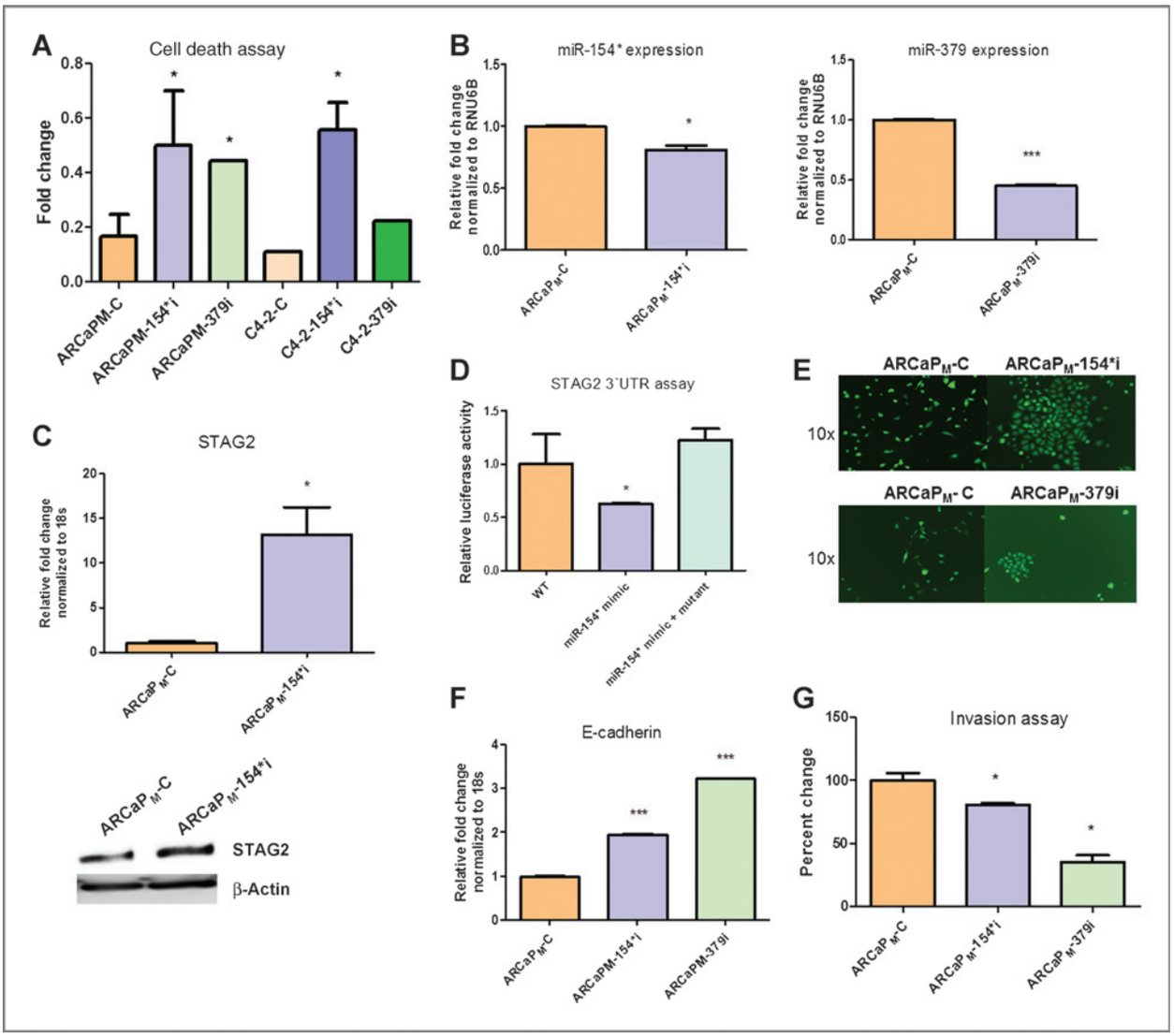

Figure 2. Inhibition of miR-154* or miR-379 results in MET of prostate cancer cells. A, cell death in ARCaP$_M$ prostate cancer cells in response to a miR-154* and miR-379 inhibitor using trypan blue exclusion assay. B, expression of miR-154* and miR-379 assayed by qRT-PCR in ARCaP$_M$-C control prostate cancer cells and ARCaP$_M$-154*i (miR-154* inhibitor transfected cells) and ARCaP$_M$-379i (miR-379 inhibitor) transfected cells. Data are normalized to RNU6B. C, STAG2 (mir-154* target) protein and mRNA expression in ARCaP$_M$-C and ARCaP$_M$-154*i prostate cancer cells assayed by Western analysis and qRT-PCR. D, 3′UTR binding luciferase assay using WT and mutant 3′UTR (STAG2) construct and miR-154* mimics in 293T cells. E, morphologic changes in ARCaP$_M$-154*i and ARCaP$_M$-379i compared with ARCaP$_M$-C control prostate cancer cells. F, E-cadherin mRNA assayed in ARCaP$_M$-C, ARCaP$_M$-154*I, and ARCaP$_M$-379i expressing prostate cancer cells by qRT-PCR, normalized to 18s RNA. G, invasion assay of ARCaP$_M$-C, ARCaP$_M$-154*I, and ARCaP$_M$-379i expressing prostate cancer cells. *, $P < 0.05$ or ***, $P < 0.001$ were considered to be statistically significant by *t* test or ANOVA–Tukey test.

increases in E-cadherin mRNA expression in ARCaP$_M$-154*i and ARCaP$_M$-379i cells but not in ARCaP$_M$-C cells (Fig. 2F). To determine if functional reversal of EMT (MET) occurred in addition to morphologic changes, we performed invasion assays on these cell lines. ARCaP$_M$-154*i and ARCaP$_M$-379i cells had significantly decreased invasive capacity compared with ARCaP$_M$-C cells (Fig. 2G). Taken together, these results demonstrate that miR-154* and miR-379 play an important role in the EMT and invasive capacity of prostate cancer cells.

Inhibition of miR-154* results in decreased bone and soft tissue metastasis of prostate cancer cells

Cancer cells gain their metastatic potential by undergoing EMT. Previous studies from our laboratory using the ARCaP model demonstrate the close association between EMT and prostate cancer bone metastasis (26). Because miR-154* levels are elevated in metastatic cancer cells, we determined whether inhibition of miR-154* would lead to decreased metastasis *in vivo*. Consistent with our hypothesis, we found that inhibition of miR-

154* resulted in increased cell death, mesenchymal to epithelial transition (MET), and decreased invasion *in vitro*. To determine if miR-154* plays a role in cancer metastasis *in vivo*, we inoculated luciferase-tagged ARCaP$_M$-C control cells or ARCaP$_M$-154*i (miR-154* inhibited) cells via the intracardiac route into SCID/Beige mice ($N = 5$/group) to mimic *in vivo* metastasis. Tumor growth was monitored by luciferase imaging. Mice that received ARCaP$_M$-154*i cells had a significantly decreased incidence of metastasis (0/5) compared with mice that received ARCaP$_M$-C control cells (4/5) at 15 weeks postinoculation. X-ray and luciferase imaging of representative mice from both groups are shown in Fig. 3A. The tumors were detected by IR783 (NIR dye) in all mice (Fig. 3A, right panels). The control mice developed metastatic tumors at 1 to 5 sites in the body, whereas ARCaP$_M$-154*i–injected mice did not develop any tumors. Bone tumors sites included the tibia, femur, humerus, and mandible, and had mixed osteoblastic and osteolytic lesions (27). Mice inoculated with ARCaP$_M$-C control cells had decreased survival compared with those inoculated with ARCaP$_M$-154*i cells as shown in the Kaplan–Meier survival curve (Fig. 3B). Taken together, these studies demonstrate that miR-154* is essential for the development of bone metastasis of human prostate cancer cells and that knockdown of miR-154* reduces bone metastasis and increases the survival of mice.

Elevated expression of miR-154* and miR-379 in human prostate cancer clinical samples

We next determined the expression of miR-154* in human prostate cancer tissues using ISH and QD analysis. miR-154* probes were biotin-labeled (Exiqon) and further labeled to a streptavidin-conjugated QD at a specified wavelength. The

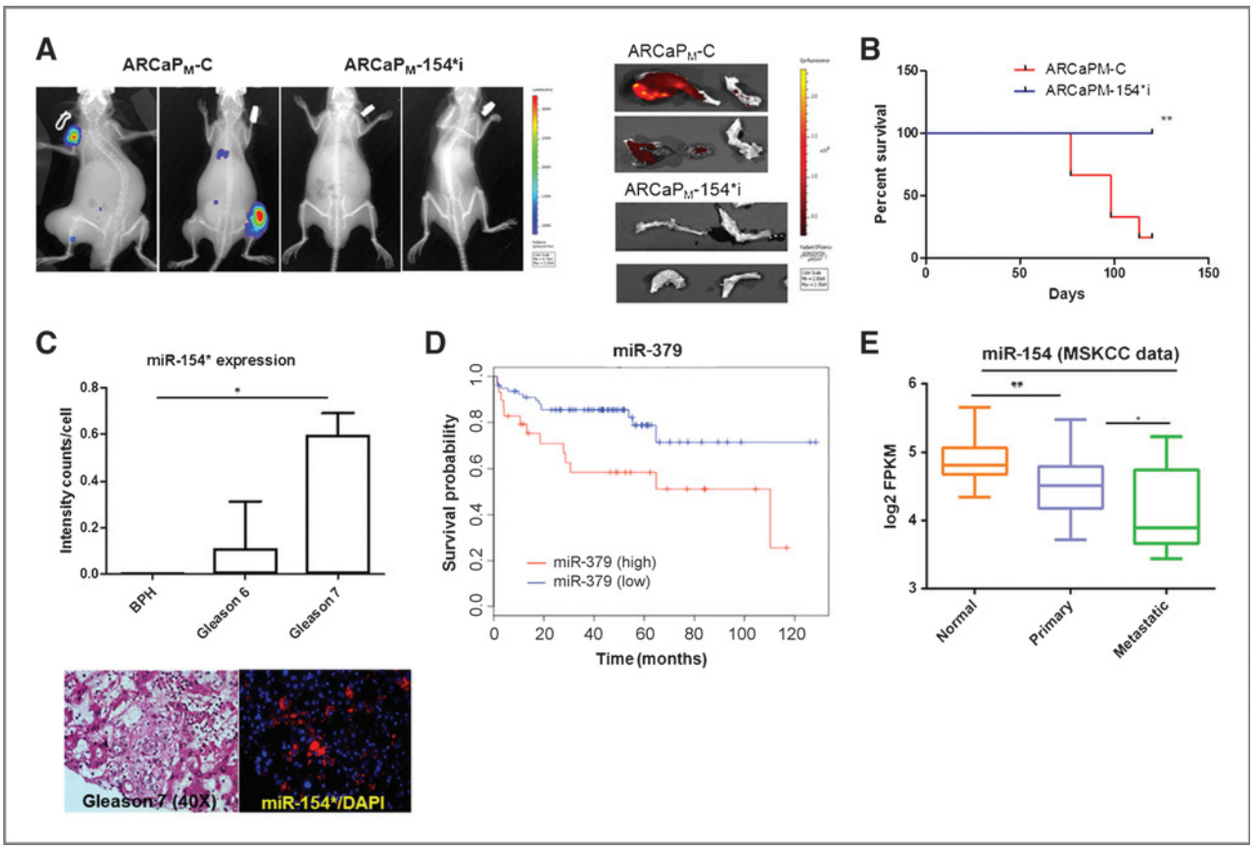

Figure 3. Inhibition of miR-154* results in decreased metastasis of bone and soft tissue of prostate cancer cells. A, representative metastatic lesions observed by X-ray/luciferase imaging of ARCaP$_M$-C cell and ARCaP$_M$-154*i cell tumors in SCID/Beige mice ($n = 5$/group) following intracardial injection. Images of bone with tumor in the ARCaP$_M$-C cells and ARCaP$_M$-154*i–injected mice using near infra-red dye (IR783). B, Kaplan–Meier curve of ARCaP$_M$-C cells and ARCaP$_M$-154*i–injected SCID/Beige mice ($n = 5$/group). C, miR-154* expression in prostate cancer clinical samples from BPH, Gleason 6 and 7 tissues assayed by ISH-QD labeling. Data were plotted as intensity counts/cell in tissues. Representative image of Gleason 7 tissue with miR-154* staining in red (magnification, ×40). Nuclei stained by DAPI. D, Kaplan–Meier disease-free survival (DFS) curves for the patients with prostate cancer, based on miR-379 expression in the MSKCC dataset. The *y*-axis is disease-free survival probability, and the *x*-axis is survival in months. Blue line represents the DFS of patients with miR-379 lower than the median of the normal individuals ($n = 78$). Red line represents the DFS of patients with miR-379 higher than the median of the normal individuals ($n = 29$). Data were analyzed using log-rank test ($P = 0.0117$). E, miR-154 expression in normal, primary, and metastatic prostate cancer patients. Significant differential expression of miR-154 was noted between normal individual ($n = 29$), primary ($n = 99$), and metastatic ($n = 14$) prostate cancer patients. *, $P < 0.05$ or **, $P < 0.005$ were considered to be statistically significant by *t* test or ANOVA–Tukey test.

tissues were separated into three groups, BPH ($N = 4$), Gleason 6 ($N = 12$), and Gleason 7 ($N = 7$). Each tissue sample has two sections. Gleason 7 tumor tissues had significantly higher staining of miR-154* compared with BPH (Fig. 3C). A representative image of Gleason 7 demonstrates higher staining in the tumor tissues (Fig. 3C). We also determined the expression of miR-154* in other cancers and found increased expression in other urological cancers (Supplementary Fig. S1). Using the publicly available database (MSKCC), we demonstrated that elevated expression of miR-379 is associated with progression-free survival and miR-154 (the opposite strand of miR-154*) is downregulated in both primary and metastatic prostate cancer tissues compared with normal individuals (Fig. 3D and E; refs. 28–30). These results are consistent with previous studies demonstrating that miR-154 is decreased in prostate cancer cell lines and clinical samples (28–30). These databases did not have information on miR-154*. Nevertheless, our observations in bone metastatic prostate cancer cell line models are clinically relevant and our experimental observations correlated well with tumor progression. These results collectively demonstrate that miR-154* and miR-379 are highly expressed in prostate cancer and miR-379 expression correlates with progression-free survival in patients.

Overexpression of miRNA members of the DLK1-DIO3 cluster promotes EMT in prostate cancer cells

Previously published studies by our lab demonstrate that miR-409-3p/5p, two key miRNAs in the DLK1-DIO3 cluster, are elevated in prostate cancer cells (12). Because all four members (miR-409-3p/5p, miR-154*, and miR-379) of the DLK1-DIO3 cluster are elevated in prostate cancer bone metastatic cells, we stably transduced ARCaP$_E$ cells, a marginally metastatic epithelial cell line, using a lentivirus that carries a GFP control vector (ARCaP$_E$-C) or a lentiviral overexpression vector that carries GFP and a combination of all four miRNAs—miR-409-3p, -5p, miR-154*, and miR-379 (ARCaP$_E$-cluster overexpression). The miRNA expression of the members of the DLK1-DIO3 cluster was determined by qRT-PCR assay (Fig. 4A). In the ARCaP$_E$ -cluster overexpression cells, miR-409-5p and miR-154* were highly expressed (100-fold) followed by moderate

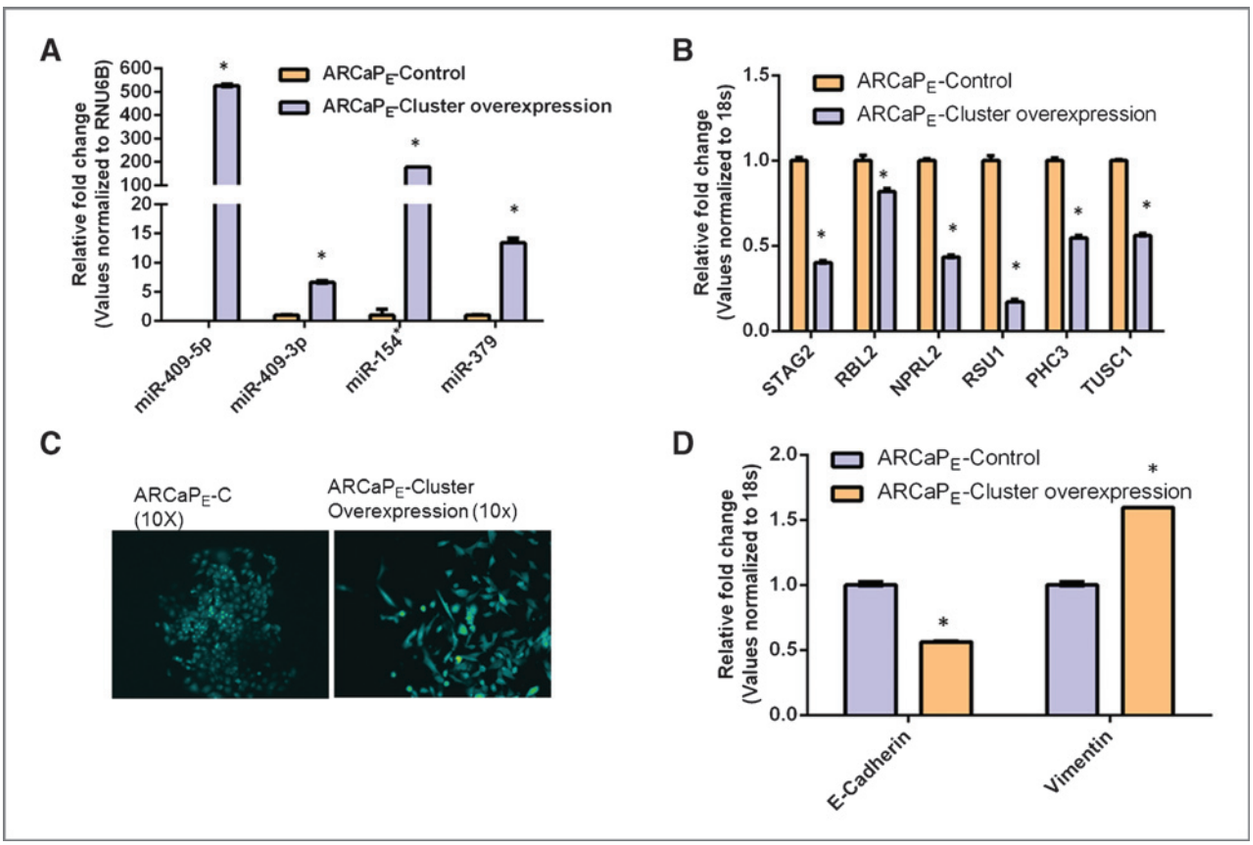

Figure 4. Overexpression of miR-154*, miR-409-3p/-5p, and miR-379 induces EMT in prostate cancer cells. A, expression of miR-409-5p/-3p, miR-154*, and miR-379 assayed by real-time PCR in ARCaP$_E$-C control prostate cancer cells and ARCaP$_E$-cluster overexpressing cells normalized to RNU6B. B, RNA expression of miR-409-5p/-3p and miR-154* targets in ARCaP$_M$ prostate cancer cells assayed by qRT-PCR (miR-154* mRNA targets: STAG2; miR-409-5p mRNA targets: STAG2, RBL2, NPRL2, and RSU1; miR-409-3p mRNA targets: RSU1, PHC3, and TUSC1). C, morphologic EMT changes in ARCaP$_E$-C control prostate cancer cells and ARCaP$_E$-cluster overexpressing cells; magnification, ×10. D, RNA expression of EMT markers, E-cadherin, and vimentin in ARCaP$_E$-C control prostate cancer cells and ARCaP$_E$-cluster overexpressing cells assayed by qRT-PCR. *, $P < 0.05$ was considered to be statistically significant by *t* test.

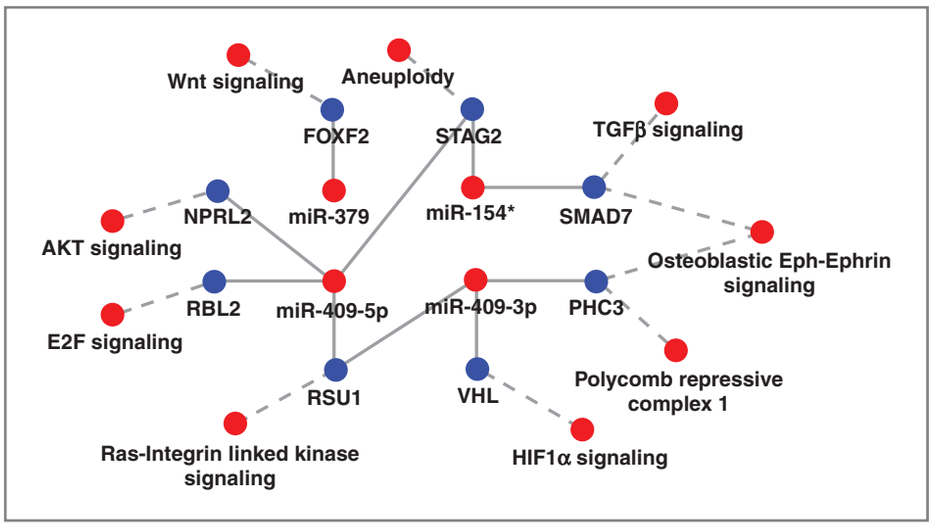

Figure 5. Cytoscape analysis of target genes and signaling pathways altered by miR-409-3p/5p, miR-154*, and miR-379 in the DLK1-DIO3 cluster. The miRNAs in this cluster target tumor suppressors which block several pathways in human cancer. Red dots represent activation of miRNA and oncogenic pathways and blue dots represent inhibition of tumor suppressor genes.

expression of miR-379 and miR-409-3p (5- to 10-fold) when compared with $ARCaP_E$-C prostate cancer cells (Fig. 4A). Next, we measured the expression levels of the target genes of these miRNAs by qRT-PCR. Several of the target genes of these four miRNAs include tumor suppressors that are shared by these miRNAs (Prediction software: Targetscan v6.2 June 2012 and Pictar). Overexpression of these miRNAs resulted in a decrease in mRNA levels of several of the target genes that are commonly shared by these miRNAs. STAG2 (target gene of miR-154* and miR-409-5p) and Ras suppressor protein 1 (RSU1; target gene of miR-409-3p and miR-409-5p) were significantly decreased in the $ARCaP_E$-cluster overexpression cells compared with control (Fig. 4B). miR-409-5p targets, including STAG2, retinoblastoma-like 2 (RBL2), nitrogen permease regulator-like 2 (NPRL2), and RSU1, were decreased in the cluster overexpression cells (Fig. 4B). Targets of miR-409-3p, including RSU1, polyhomeotic homolog 3 (PHC3), and tumor suppressor candidate 1 (TUSC1), were decreased in cluster overexpression cells (Fig. 4B). These results demonstrate that overexpression of miRNA members of the DLK1-DIO3 miRNA mega-cluster results in decreased expression of several tumor suppressor genes. We also observed EMT changes in $ARCaP_E$-cluster overexpression prostate cancer cells. The cells appeared spindle shaped and had decreased expression of E-cadherin and increased expression of vimentin compared with $ARCaP_E$-C cells (Fig. 4C). To evaluate the combinatorial effects of knockdown of all four miRNAs (miR-409-3p, miR-409-5p, miR-379, and miR-154*) in metastatic $ARCaP_M$ prostate cancer cells, we introduced shRNA that targets all four miRNAs and found that successful shRNA-mediated knockdown of miR-154* and miR-409-3p (the knockdown of miR-409-5p and miR-379 was not effective in this experiment) led to reversal of EMT. $ARCaP_M$ cells underwent morphologic, biochemical, and functional EMT changes upon knockdown of miR-154* and miR-409-3p (Supplementary Fig. S2A–S2D).

Analyses of the target pathways regulated by these miRNAs include oncogenic pathways such as E2F signaling, the Ras pathway, hypoxia inducible factor signaling, and the WNT and TGFβ pathways. These pathways also activate EMT and the cancer stem cell phenotype (Fig. 5). miR-154* targets STAG2 and SMAD7. STAG2 is known to induce aneuploidy (25, 31). SMAD7 is an inhibitor of the TGFβ pathway (32). miR-379 is predicted to inhibit forkhead box F2 (FOXF2), which has been shown to inhibit the WNT pathway in colon cancer development (33). We previously demonstrated that miR-409-3p and miR-409-5p inhibit RSU1, which is a known inhibitor of the oncogenic Ras pathway (12, 34, 35). Other targets of miR-409-3p include von Hippel–Lindau (VHL) tumor suppressor, E3 ubiquitin protein ligase, and PHC3. VHL is a tumor suppressor and degrades HIF1α (36). Inhibition of VHL results in the stabilization of HIF1α, which is known to induce resistance to radiation and chemotherapeutic agents (37). PHC3 is a tumor suppressor protein and is lost in osteosarcoma (38). PHC3 and ephrin receptors have been predicted to exhibit protein–protein interactions (www.biograph.be/). miR-409-5p has been shown to target STAG2, RSU1, NPRL2, and RBL2 (12). NPRL2 activates AKT pathway (39, 40) and RBL2 activates the E2F pathway (41). Thus, these miRNAs activate oncogenic proteins by targeting tumor suppressors. Because these miRNAs are elevated in prostate cancer bone metastatic models, we determined the levels of these miRNAs in human prostate cancer bone metastatic samples using multiplexed ISH-QD labeling. We observed increased miR-154*, miR-409-3p, and miR-409-5p staining in human metastatic tumor tissues in the bone (Fig. 6). Taken together, these results demonstrate that miR-154*, miR-409-3p/-5p, and miR-379 induce EMT in prostate cancer cells, show upregulated expression in human prostate cancer bone metastasis tissues, and correlate with progression-free survival in patients with prostate cancer.

Discussion

To understand the biology of the miRNAs of the DLK1-DIO3 mega-cluster in EMT and cancer bone metastasis and

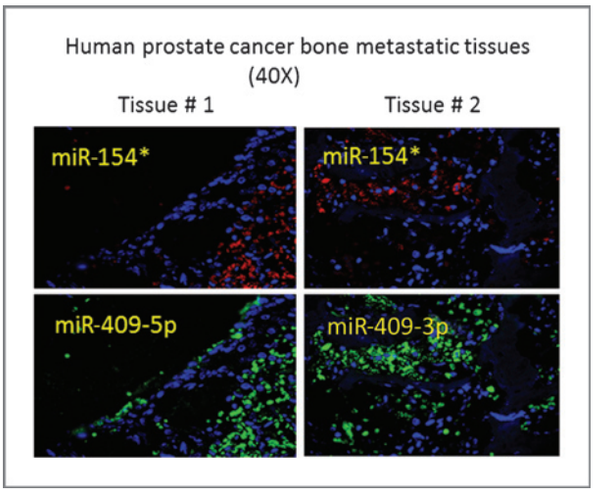

Figure 6. miR-154* (red), miR-409-3p (green), and miR-409-5p (green) staining of human prostate bone metastatic tissue using multiplexed ISH-QD labeling. Two human prostate bone metastatic tissues were used, and multiplexed for probes against miR-154* and miR-409-3p or miR-409-5p.

to identify novel biomarkers and/or therapeutic targets, we probed for specific miRNAs of this mega-cluster in unique EMT models of human prostate cancer developed in our laboratory. Specifically, the miRNAs miR-154* and miR-379, located within the DLK1-DIO3 cluster, were highly upregulated in two prostate cancer cell lines with a mesenchymal phenotype and with bone metastatic potential (Fig. 1). The miRNA members of the DLK1-DIO3 cluster have been shown to be important for totipotency during embryogenesis and induced pluripotent stem cell formation. We uncovered a surprising role for miR-154* and miR-379, which is expressed by embryonic stem cells and pluripotent stem cells, promoting prostate cancer development and metastasis. Specifically, we show that (i) miR-154* and miR-379 are elevated in human prostate cancer tumor tissues and miR-379 expression correlates with progression-free survival of patients with prostate cancer, (ii) miR-154* and miR-379 can promote EMT of prostate cancer cells *in vitro*, and (iii) inhibition of miR-154* results in decreased bone metastatic tumor growth and increased survival. Thus, miR-154* and miR-379 appear to be promising new biomarkers for cancer detection and attractive new therapeutic targets for prostate cancer treatment.

The primary functions of miR-154* are to repress tumor suppressors and modulate the expression of EMT and stemness to mediate downstream convergent signal axes. Inhibition of miR-154* resulted in increased E-cadherin and decreased invasion *in vitro*. miR-154*-depleted prostate cancer cells had decreased bone metastasis and increased survival. miR-154* mediates its effects by downregulating its target gene, STAG2, which is a tumor suppressor. STAG2 plays a critical role in the cohesion complex, and a decrease in STAG2 has been correlated with aneuploidy and cancer (25, 31). Other miR-154* target genes may be involved such as SMAD7, which inhibits the TGFβ pathways (32) involved in EMT (42). Interestingly, the sense strand of miR-154* is undetectable or decreased in prostate cancer models and in patients with prostate cancer (28, 29, 30). miR-154* is upregulated in both patients with lung squamous cell carcinoma and lung adenocarcinoma (9). miR-379, another member of the DLK1-DIO3 cluster, located upstream of the miR-154 gene cluster, is moderately elevated in prostate cancer cells (Fig. 1). Inhibition of miR-379 also resulted in reversal of EMT (MET), increased E-cadherin, and decreased invasion. miR-379 expression in clinical specimens correlates with disease-free survival of patients with prostate cancer. Consistent with our observations, previous reports demonstrate that the miRNAs of the DLK1-DIO3 cluster are elevated in the serum of patients with cancer compared with healthy patients (9, 11). Accordingly, it was shown that miR-379 is also elevated in patients with metastatic prostate cancer compared with patients with localized disease (43). Interestingly, other members of the DLK1-DIO3 mega-cluster share similar mRNA target genes. STAG2 is targeted by both miR-154* and miR-409-5p, whereas RSU1 is targeted by both miR-409-5p and miR-409-3p. Thus, the members of the cluster work synergistically and are elevated in the mesenchymal-type prostate cancer cells to promote EMT and metastasis (Fig. 5). We conclude that the miRNA members of the DLK1-DIO3 cluster promote EMT, stemness, and bone metastasis in prostate cancer. These findings have potential clinical implications in both the biomarker field and the therapeutic arena.

Disclosure of Potential Conflicts of Interest

No potential conflicts of interest were disclosed.

Authors' Contributions

Conception and design: M. Gururajan, S. Josson, E.M. Posadas, L.W.K. Chung

Development of methodology: M. Gururajan, S. Josson, H.E. Zhau, C. Liu, L.W.K. Chung

Acquisition of data (provided animals, acquired and managed patients, provided facilities, etc.): M. Gururajan, S. Josson, G.C.-Y. Chu, C.L. Haga, J. Lichterman, P. Duan, E.M. Posadas, L.W.K. Chung

Analysis and interpretation of data (e.g., statistical analysis, biostatistics, computational analysis): M. Gururajan, S. Josson, C.-L. Lu, Y.-T. Lu, L.W.K. Chung

Writing, review, and/or revision of the manuscript: M. Gururajan, S. Josson, Y.-T. Lu, H.E. Zhau, J. Lichterman, E.M. Posadas, L.W.K. Chung

Administrative, technical, or material support (i.e., reporting or organizing data, constructing databases): M. Gururajan, S. Josson, C.-L. Lu, Y.-T. Lu, E.M. Posadas, L.W.K. Chung

Study supervision: M. Gururajan, S. Josson, E.M. Posadas, L.W.K. Chung

Acknowledgments

The authors thank Drs. Svendsen and Sareen for sharing the iPSC and embryonic stem cell cultures and Gary Mawyer for editing the article.

Grant support

This study was supported by grants P01-CA98912, DAMD-17-03-02-0033, and RO1-CA122602 (to L.W.K. Chung).

The costs of publication of this article were defrayed in part by the payment of page charges. This article must therefore be hereby marked *advertisement* in accordance with 18 U.S.C. Section 1734 solely to indicate this fact.

Received July 11, 2014; revised October 2, 2014; accepted October 9, 2014; published OnlineFirst October 16, 2014.

References

1. Wellner U, Schubert J, Burk UC, Schmalhofer O, Zhu F, Sonntag A, et al.The EMT-activator ZEB1 promotes tumorigenicity by repressing stemness-inhibiting microRNAs. Nat Cell Biol 2009;11:1487–95.
2. Liu C, Kelnar K, Liu B, Chen X, Calhoun-Davis T, Li H, et al.The microRNA miR-34a inhibits prostate cancer stem cells and metastasis by directly repressing CD44. Nat Med 2011;17:211–5.
3. Han Z, He H, Zhang F, Huang Z, Liu Z, Jiang H, et al.Spatiotemporal expression pattern of Mirg, an imprinted non-coding gene, during mouse embryogenesis. J Mol Histol 2012;43:1–8.
4. Lim L, Balakrishnan A, Huskey N, Jones KD, Jodari M, Ng R, et al.MiR-494 within an oncogenic MicroRNA megacluster regulates G1/S transition in liver tumorigenesis through suppression of MCC. Hepatology 2014;59:202–15
5. Luk JM, Burchard J, Zhang C, Liu AM, Wong KF, Shek FH, et al.DLK1-DIO3 genomic imprinted microRNA cluster at 14q32.2 defines a stem-like subtype of hepatocellular carcinoma associated with poor survival. J Biol Chem 2011;286:30706–13.
6. Haga CL, Phinney DG. MicroRNAs in the imprinted DLK1-DIO3 region repress the epithelial-to-mesenchymal transition by targeting the TWIST1 protein signaling network. J Biol Chem 2012;287:42695–707.
7. Lempiainen H, Couttet P, Bolognani F, Muller A, Dubost V, Luisier R, et al.Identification of Dlk1-Dio3 imprinted gene cluster noncoding RNAs as novel candidate biomarkers for liver tumor promotion. Toxicol Sci 2013;131:375–86.
8. Valdmanis PN, Roy-Chaudhuri B, Kim HK, Sayles LC, Zheng Y, Chuang CH, et al.Upregulation of the microRNA cluster at the Dlk1-Dio3 locus in lung adenocarcinoma. Oncogene 2013 Dec 9. [Epub ahead of print].
9. Cazzoli R, Buttitta F, Di Nicola M, Malatesta S, Marchetti A, Rom WN, et al.microRNAs derived from circulating exosomes as noninvasive biomarkers for screening and diagnosing lung cancer. J Thorac Oncol 2013;8:1156–62.
10. Li S, Meng H, Zhou F, Zhai L, Zhang L, Gu F, et al.MicroRNA-132 is frequently down-regulated in ductal carcinoma in situ (DCIS) of breast and acts as a tumor suppressor by inhibiting cell proliferation. Pathol Res Pract 2013;209:179–83.
11. Nguyen HC, Xie W, Yang M, Hsieh CL, Drouin S, Lee GS, et al. Expression differences of circulating microRNAs in metastatic castration resistant prostate cancer and low-risk, localized prostate cancer. Prostate 2013;73:346–54.
12. Josson S, Gururajan M, Hu P, Shao C, Chu GC, Zhau HE, et al.miR-409–3p/-5p promotes tumorigenesis, epithelial to mesenchymal transition and bone metastasis of human prostate cancer. Clin Cancer Res 2014;20:4636–46.
13. Xu J, Wang R, Xie ZH, Odero-Marah V, Pathak S, Multani A, et al. Prostate cancer metastasis: role of the host microenvironment in promoting epithelial to mesenchymal transition and increased bone and adrenal gland metastasis. Prostate 2006;66:1664–73.
14. Thalmann GN, Sikes RA, Wu TT, Degeorges A, Chang SM, Ozen M, et al.LNCaP progression model of human prostate cancer: androgen-independence and osseous metastasis. Prostate 2000;44:91–103.
15. Josson S, Sung SY, Lao K, Chung LW, Johnstone PA. Radiation modulation of microRNA in prostate cancer cell lines. Prostate 2008;68:1599–606.
16. Taylor BS, Schultz N, Hieronymus H, Gopalan A, Xiao Y, Carver B, et al. Integrative genomic profiling of human prostate cancer. Cancer Cell 2010;18:11–22.
17. Gao J, Aksoy BA, Dogrusoz U, Dresdner G, Gross B, Sumer SO, et al. Integrative analysis of complex cancer genomics and clinical profiles using the cBioPortal. Sci Sig 2013;6:pl1.
18. Nomura T, Huang WC, Zhau HE, Wu D, Xie Z, Mimata H, et al.Beta2-microglobulin promotes the growth of human renal cell carcinoma through the activation of the protein kinase A, cyclic AMP-responsive element-binding protein, and vascular endothelial growth factor axis. Clin Cancer Res 2006;12:7294–305.
19. Hu P, Chu GC, Zhu G, Yang H, Luthringer D, Prins G, et al.Multiplexed quantum dot labeling of activated c-Met signaling in castration-resistant human prostate cancer. PloS ONE 2011;6:e28670.
20. Josson S, Nomura T, Lin JT, Huang WC, Wu D, Zhau HE, et al.beta2-microglobulin induces epithelial to mesenchymal transition and confers cancer lethality and bone metastasis in human cancer cells. Cancer Res 2011;71:2600–10.
21. Thalmann GN, Anezinis PE, Chang SM, Zhau HE, Kim EE, Hopwood VL, et al.Androgen-independent cancer progression and bone metastasis in the LNCaP model of human prostate cancer. Cancer Res 1994;54:2577–81.
22. Liu L, Luo GZ, Yang W, Zhao X, Zheng Q, Lv Z, et al.Activation of the imprinted Dlk1-Dio3 region correlates with pluripotency levels of mouse stem cells. J Biol Chem 2010;285:19483–90.
23. Stadtfeld M, Apostolou E, Akutsu H, Fukuda A, Follett P, Natesan S, et al.Aberrant silencing of imprinted genes on chromosome 12qF1 in mouse induced pluripotent stem cells. Nature 2010;465:175–81.
24. Huang WC, Wu D, Xie Z, Zhau HE, Nomura T, Zayzafoon M, et al.beta2-microglobulin is a signaling and growth-promoting factor for human prostate cancer bone metastasis. Cancer Res 2006;66:9108–16.
25. Solomon DA, Kim T, Diaz-Martinez LA, Fair J, Elkahloun AG, Harris BT, et al.Mutational inactivation of STAG2 causes aneuploidy in human cancer. Science 2011;333:1039–43.
26. Zhau HE, Odero-Marah V, Lue HW, Nomura T, Wang R, Chu G, et al. Epithelial to mesenchymal transition (EMT) in human prostate cancer: lessons learned from ARCaP model. Clin Exp Metastasis 2008;25: 601–10.
27. Odero-Marah VA, Wang R, Chu G, Zayzafoon M, Xu J, Shi C, et al. Receptor activator of NF-kappaB Ligand (RANKL) expression is associated with epithelial to mesenchymal transition in human prostate cancer cells. Cell Res 2008;18:858–70.
28. Formosa A, Markert EK, Lena AM, Italiano D, Finazzi-Agro E, Levine AJ, et al.MicroRNAs, miR-154, miR-299–5p, miR-376a, miR-376c, miR-377, miR-381, miR-487b, miR-485–3p, miR-495 and miR-654–3p, mapped to the 14q32.31 locus, regulate proliferation, apoptosis, migration and invasion in metastatic prostate cancer cells. Oncogene 2013 Oct 28. [Epub ahead of print].
29. Zhu C, Li J, Cheng G, Zhou H, Tao L, Cai H, et al.miR-154 inhibits EMT by targeting HMGA2 in prostate cancer cells. Mol Cell Biochem 2013;379:69–75.
30. Zhu C, Shao P, Bao M, Li P, Zhou H, Cai H, et al.miR-154 inhibits prostate cancer cell proliferation by targeting CCND2. Urol Oncol 2014;32:31.e9–16.
31. Kim MS, Kim SS, Je EM, Yoo NJ, Lee SH. Mutational and expressional analyses of STAG2 gene in solid cancers. Neoplasma 2012;59:524–9.
32. Edlund S, Bu S, Schuster N, Aspenstrom P, Heuchel R, Heldin NE, et al. Transforming growth factor-beta1 (TGF-beta)-induced apoptosis of prostate cancer cells involves Smad7-dependent activation of p38 by TGF-beta-activated kinase 1 and mitogen-activated protein kinase kinase 3. Mol Biol Cell 2003;14:529–44.
33. Nik AM, Reyahi A, Ponten F, Carlsson P. Foxf2 in intestinal fibroblasts reduces numbers of Lgr5(+) stem cells and adenoma formation by inhibiting Wnt signaling. Gastroenterology 2013;144:1001–11.
34. Gonzalez-Nieves R, Desantis AI, Cutler ML. Rsu1 contributes to regulation of cell adhesion and spreading by PINCH1-dependent and - independent mechanisms. J Cell Commun Signal 2013;7:279–93
35. Dougherty GW, Jose C, Gimona M, Cutler ML. The Rsu-1-PINCH1-ILK complex is regulated by Ras activation in tumor cells. Eur J Cell Biol 2008;87:721–34.
36. Maxwell PH, Wiesener MS, Chang GW, Clifford SC, Vaux EC, Cockman ME, et al.The tumour suppressor protein VHL targets hypoxia-inducible factors for oxygen-dependent proteolysis. Nature 1999;399: 271–5.
37. Palayoor ST, Burgos MA, Shoaibi A, Tofilon PJ, Coleman CN. Effect of radiation and ibuprofen on normoxic renal carcinoma cells overexpressing hypoxia-inducible factors by loss of von Hippel-Lindau tumor suppressor gene function. Clin Cancer Res 2004;10:4158–64.
38. Iwata S, Takenobu H, Kageyama H, Koseki H, Ishii T, Nakazawa A, et al.Polycomb group molecule PHC3 regulates polycomb complex composition and prognosis of osteosarcoma. Cancer Sci 2010; 101:1646–52.

39. Kurata A, Katayama R, Watanabe T, Tsuruo T, Fujita N. TUSC4/NPRL2, a novel PDK1-interacting protein, inhibits PDK1 tyrosine phosphorylation and its downstream signaling. Cancer Sci 2008;99:1827–34.
40. Bar-Peled L, Chantranupong L, Cherniack AD, Chen WW, Ottina KA, Grabiner BC, et al.A Tumor suppressor complex with GAP activity for the Rag GTPases that signal amino acid sufficiency to mTORC1. Science 2013;340:1100–6.
41. Maddika S, Ande SR, Panigrahi S, Paranjothy T, Weglarczyk K, Zuse A, et al.Cell survival, cell death and cell cycle pathways are interconnected: implications for cancer therapy. Drug Resist Updat 2007;10:13–29.
42. Lenferink AE, Cantin C, Nantel A, Wang E, Durocher Y, Banville M, et al.Transcriptome profiling of a TGF-beta-induced epithelial-to-mesenchymal transition reveals extracellular clusterin as a target for therapeutic antibodies. Oncogene 2010;29:831–44.
43. Bryant RJ, Pawlowski T, Catto JW, Marsden G, Vessella RL, Rhees B, et al.Changes in circulating microRNA levels associated with prostate cancer. Br J Cancer 2012;106:768–74.